Journal Pre-proof

Development of an integrated model for prediction of impact and vibration response of hybrid fiber metal laminates with a viscoelastic layer

Hui Li , Zelin Li , Zhengyang Xiao , Xiangping Wang , Jian Xiong , Jin Zhou , Zhongwei Guan

PII: S0020-7403(21)00033-3
DOI: https://doi.org/10.1016/j.ijmecsci.2021.106298
Reference: MS 106298

To appear in: *International Journal of Mechanical Sciences*

Received date: 18 October 2020
Revised date: 24 December 2020
Accepted date: 19 January 2021

Please cite this article as: Hui Li , Zelin Li , Zhengyang Xiao , Xiangping Wang , Jian Xiong , Jin Zhou , Zhongwei Guan , Development of an integrated model for prediction of impact and vibration response of hybrid fiber metal laminates with a viscoelastic layer, *International Journal of Mechanical Sciences* (2021), doi: https://doi.org/10.1016/j.ijmecsci.2021.106298

Highlights

- An integrated dynamic model is developed to predict the coupled impact and vibration behavior of a FML plate structure with a viscoelastic layer
- A predefined the damage criterion based on a key indicator “critical impact velocity”, is proposed to estimate whether the hybrid composite structure is damaged subjected to different low-velocity impact excitations
- A solid validation of the model developed is conducted via a series of dynamic experiments with different impact velocities
- Material and geometrical parameters are discussed to improve the structural vibration and impact resistant capabilities

Development of an integrated model for prediction of impact and vibration response of hybrid fiber metal laminates with a viscoelastic layer

Hui Li[a, b, c], Zelin Li[a], Zhengyang Xiao[a], Xiangping Wang[b], Jian Xiong[d, *], Jin Zhou[e], Zhongwei Guan[c,f]

[a] School of Mechanical Engineering and Automation, Northeastern University, Shenyang 110819, China
[b] Key Laboratory of Impact Dynamics on Aero Engine, Shenyang 110015, China
[c] School of Engineering, University of Liverpool, Brownlow Street, Liverpool L69 3GQ, United Kingdom
[d] Center for Composite Materials and Structures, Harbin Institute of Technology, Harbin 150001, China
[e] School of Mechanical Engineering，Xi'an Jiaotong University，Xi'an 710054，China
[f] Technology Innovation Institute, Masdar City, Abu Dhabi, UAE

* Corresponding author, Tel.:+86 0451 86402736.
E-mail address: jx@hit.edu.cn (Professor Jian Xiong).

Graphical Abstract

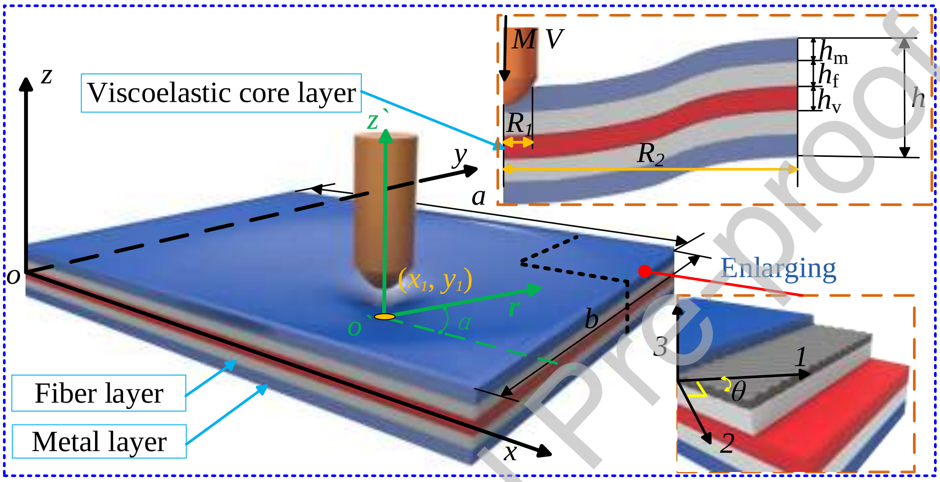

Abstract: The present study proposes an integrated model for prediction of the dynamic behaviors involving vibration and impact on hybrid fiber metal laminates embedded with a viscoelastic layer. Firstly, by combining the Reddy's high-order shear deformation theory and the classical laminate theory, the structural displacement field functions are determined. Then, a predefined criterion, namely the damage criterion based on a key indicator "critical impact velocity", is proposed to quantitatively estimate whether the composite structure is damaged subjected to impact excitation. In the case that meets this criterion without considering impact damage, the energy method, together with the Duhamel principle and the Simpson numerical integral approach, is utilized to obtain the free and forced vibration solutions. However, in the case that fails to satisfy this criterion, by applying the progressive quasi-static approach, the key impact parameters which include critical the impact contact force and displacement are successfully solved. Some numerical results provided in the literature are utilized to give initial validation of the model. Additionally, the detailed experimental tests are performed on the hybrid plate specimens to further validate the model developed. Using the validated model, the effects of the thickness ratio of the viscoelastic layer to the overall plate and Young's moduli of the viscoelastic layer on the dynamic responses are discussed. The outputs provide important references for this type of composite hybrid structures with improving the anti-vibration and impact resistant capabilities.

Keywords: Hybrid fiber metal laminates; Viscoelastic layer; Load-displacement curve; Impact and vibration response; Critical impact velocity

Author Statement

Hui Li: Conceptualization, Methodology, Writing- Original draft preparation

Zelin Li: Formal analysis, Software, Programming

Zhengyang Xiao: Visualization, Programming

Xiangping Wang: Investigation, Supervision

Jian Xiong: Conceptualization, Methodology, Writing - Review & Editing, Supervision

Jin Zhou: Methodology, Validation

Zhongwei Guan: Investigation, Validation

1. Introduction

Fiber metal laminates (FMLs) have been increasingly applied in the aerospace, shipbuilding and other industries [1-2]. For example, fan blades in aeroengine, solar panel in satellites and body skin parts, vertical and horizontal tail leading edges, rectifying panels in military and civil aircrafts [3-4], etc. As FML structures are often working in the complex environments and load conditions, such as bird and hailstone impact, runway debris and tool collisions, there are often reported cases on the severe vibration phenomena led by spinning imbalance loads, the continuously reduced stiffness and strength caused by dynamic loads and serious impact accidents [5-7]. Viscoelastic damping (VR) material has been found to possess the excellent passive damping capability with many advantages such as easy to manufacture, anti-aging and low-cost. If the VR material can be embedded into FMLs (e.g. as a core layer), the vibration, impact, noise resistance properties of the whole laminated structure can be greatly improved [8]. Therefore, it is necessary to study this new type of FMLs through the theoretical and numerical modeling, failure mechanism analysis and experimental work.

For the past a few decades, the extensive studies have been conducted on impact or vibration characteristics of FML structures separately, where various modeling and analysis approaches were developed. For example, Vlot [9] firstly proposed an analytical model to determine the impact response of FMLs. After that, the important contributions [10-12] were made on improving and optimizing the analytical models to predict the contact force, displacement response, damage area, crack length and other mechanical parameters related to different impact velocities. Furthermore, Khalili [13], Shokuhfar [14], Payeganeh et al. [15] presented several theoretical models of FMLs subjected to low-velocity impact excitation via an assumption of two degrees-of-freedom spring-mass system. Guan et al. [16] predicted the variation of the maximum permanent displacement versus the normalized impact energy of FMLs based on the finite element (FE) model. Zhou et al. [17-18] investigated the effects of core layer density and aqueous environment on perforation resistance of foam-based sandwich panels by combining experimental work with numerical modelling. By regarding the low-velocity impact as a quasi-static process, Lin, Moriniere et al. [19-21] obtained the equivalent contact force functions of FML panels with a spring-mass analytical model. Based on the first order shear deformation theory, Shooshtari and Razavi [22] presented a novel vibration model of FMLs to predict the natural frequencies and transverse responses. By considering the weak bonded theory, the finite difference method and the Newmark integral method, Fu et al. [23-24] solved the dynamic response of FML structures with interfacial damage. By using a five-parameter fractional model, Iriondo et al. [25] investigated the complex moduli and loss factors of the FMLs with the self-reinforced polypropylene. Sessner et al. [26] employed the Dynamic Mechanical Analysis instrument to measure the temperature and frequency dependent damping behavior of FMLs with and without elastomer. Nassir et al. [27] predicted the maximum force and displacement, perforation energy of FMLs and also identified the failure modes by finite element analysis techniques.

Recently, researchers started to pay attention to the impact suppression issues of sandwich structures with soft material layers. Malekzadeh et al. [28] proposed an improved high-order impact theory and obtained the low-velocity impact responses of sandwich panels with flexible cores by ignoring the effect of impact damage. Shariyat and Hosseini [29] established an impact model of composite sandwich plates with viscoelastic cores. However, the effects of failure modes such as delamination, tensile fracture of fiber and matrix on the impact contact forces and energy absorption properties were not considered. To simulate the failure behavior of a composite sandwich plate subjected to impact loading, Long et al. [30] proposed a numerical model of the plate with a foam core by ignoring its fluidity. Besides the impact dynamics, several studies are also reported on the vibrations of composite laminated structures (including FMLs) with a soft material layer. Araujo et al. [31] established the finite element (FE) model of an anisotropic laminated plate with a viscoelastic core to evaluate the modal loss factors. Based on the virtual displacement principle, Azoti et al. [32] predicted the natural frequencies and loss factors of 5-layer beam structures with two auxetic viscoelastic layers. By assuming the same displacement field functions for the constituent layers, Yang et al. [33] presented a modified Fourier-Ritz solution of natural frequencies and loss factors of composite laminated plates with viscoelastic and functionally graded layers. Based on the first order shear deformation theory in conjunction with the FE method, Biswal and Mohanty [34] conducted the free vibration analysis for the multilayer sandwich shell panels with viscoelastic core. Li et al. [35] developed a nonlinear analytical model to evaluate the vibration suppression effect of a laminated plate structure with a MRE soft core accounting for both internal temperature and magnetic fields.

Up to date, the research work usually focuses on establishing dynamic models of composite laminated structures with an embedded soft material layer (or core) by only dealing with either impact or vibration problems alone. To the best of the author’s knowledge, no work has been reported on a vibro-impact modeling technology for this type of structures. There is a need to investigate both impact and vibration responses with together to pave the way for engineering applications of such the hybrid laminated structure. To deal with this problem, an integrated dynamic model is developed to predict the impact and vibration behaviors of a FML plate structure with a viscoelastic layer (so called VC-FML plate) simultaneously. A series of experimental tests are also performed to validate the theoretical model developed. Using the validated model, further investigations are undertaken to evaluate the effects of low-velocity impact excitations with different velocities on the contact force, the natural frequency and vibrational displacement. Finally, important influential factors are discussed for better exerting the impact and vibration resistance of the VC-FML plate structures.

2. Theory and formulation

2.1 Description of the model

Here, a 5-layer VC-FML plate structure with a stacking sequence of metal – composite – viscoelastic material – composite – metal is used as an example to describe the integrated modelling approach. Fig.1 displays this theoretical model for analysis of coupled impact and vibration behaviors, where a global Cartesian coordinate system *o*-*xyz* is set up at the mid-plane of the viscoelastic layer, and a local polar coordinate system $o'-r\alpha z'$ is established at the center of arbitrary impact point $o'(x_1, y_1)$. The corresponding length, width and thickness are *a*, *b* and *h*, and the thickness of the metal layer, composite layer and viscoelastic layer is denoted by h_m, h_f and h_v, respectively. Moreover, “1”, “2” and “3” are three principal directions in the composite layer, and θ denotes an angle between the direction “1” in each composite layer and the *x*-axis. In addition, *V* represents the impact velocity of an impactor with a mass of *M* when it gets into contact with the front face of the VC-FML plate, and R_1, R_2 are the radius values of the contact and stretching areas when the contact deformation is considered.

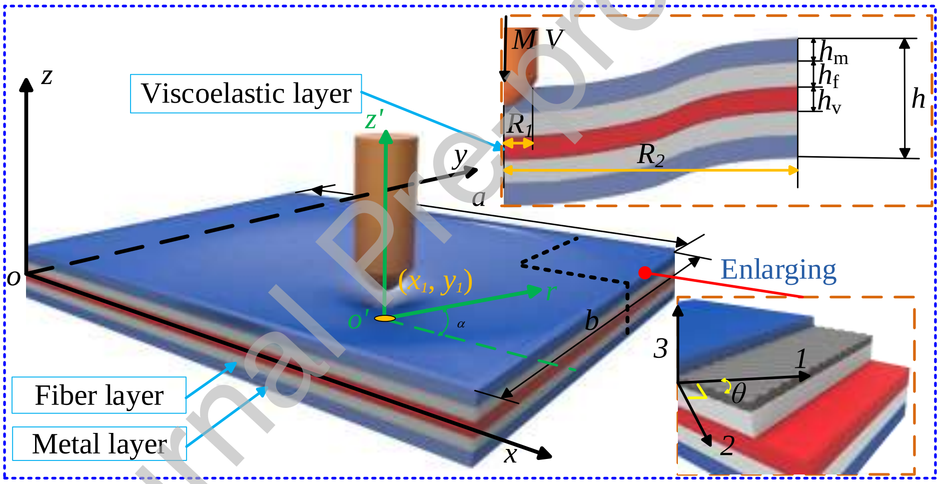

Fig.1 An integrated model of a VC-FML plate structure for analysis of the coupled impact and vibration behavior.

In the modelling process, the following assumptions need to be firstly clarified:

(1) All individual layers in the VC-FML structure are fully bonded without relative slippage;

(2) Impact load is regarded as low velocity impact force, so the strain rate effect is neglected;

(3) Impact area is assumed to be a circle with R_2 being the radius and contact point o' being the center. Therefore, the small deflection beyond this impact area is regarded as the undamaged zone;

(4) Effects of friction and impactor deformation during the impact is ignored.

2.2 Stress-strain relationships

By combining the Reddy’s high-order shear deformation theory (applied to the viscoelastic layer to account for effects of shear deformations) and the classical laminate theory (applied to the other layers), the displacement field functions of the VC-FML plate can be given as

$$\lambda(i) = \lambda(i+3) + z\lambda(i+3s) - \frac{4z^3}{3h^2}\left(\lambda(i+3s) - \lambda(i+6)\right) \ (i\text{=1, 2, 3; } s\text{=2, 3}) \tag{1}$$

where $\lambda = \left[u, v, w, u_0(x,y,t),\ v_0(x,y,t),\ w_0(x,y,t), -\frac{\partial w}{\partial x}, -\frac{\partial w}{\partial y}, 0, \varphi_x,\ \varphi_y,\ 0\right]$, s=2 represents the classical laminated theory, and s=3 represents the high-order shear deformation theory. Besides, t is the time, and φ_x and φ_y are the rotations of transverse normal in the *xz* and *yz* planes, respectively.

The structural displacements $\overline{W}$ along different directions in the Cartesian coordinate system are

$$\overline{W} = e^{i\omega t}\sum_{m=1}^{M}\sum_{n=1}^{N}\overline{w}_{mn}P_m(x)P_n(y)\left(\overline{W} = u_0,\ v_0,\ w_0^d,\ \varphi_x,\ \varphi_y\right) \tag{2}$$

where ω is the excitation frequency, $u_0, v_0, w_0^d, \varphi_x, \varphi_y$ are the displacement components, $\overline{w}_{mn} = A_{mn}, B_{mn}, C_{mn}, D_{mn}, E_{mn}$ are the unknown eigenvectors which need to be solved, $P_m(x)$ and $P_n(y)\ (m = 1,...,M;\ n = 1,...,N)$ are the orthogonal polynomials related to the fully fixed boundary conditions of four edges, and M and N are the truncation coefficients used in the Ritz method [36].

In the impact event, assume that the VC-FML plate will generate two kinds of deformed areas, namely the contact area and the stretched area, as shown in Fig.1. Thus, the displacement function w_0^p in the polar coordinate system is given by

$$w_0^p = \begin{cases} w_{\max} & 0 < r \le R_1 \\ \frac{w_{\max}v_{\mathrm{m}}}{\left(1-\frac{R_1}{R_2}\right)^4}\left(1-\frac{r}{R_2}\right)^4 + \frac{w_{\max}v_{\mathrm{f}}}{\left(1-\left(\frac{R_1}{R_2}\right)^2\right)}\left(1-\left(\frac{r}{R_2}\right)^2\right)^2 + \frac{w_{\max}v_{\mathrm{v}}}{\left(1-\frac{R_1}{R_2}\right)^4}\left(1-\frac{r}{R_2}\right)^4 & R_1 < r \le R_2 \end{cases} \tag{3}$$

where $w_{\max}$ is the maximum displacement at the impact center; v_m, v_f, v_v are the volume fractions of metal, fiber and viscoelastic layers; $R_2 = \sqrt{9FT_0 / 8w_{\max}\pi^2\left(h\tau_a\right)^2}$, of which T_0 is the impact energy, τ_a is the allowable interlaminar shear stress, and F is the impact contact force.

In addition, the displacement variable w_0 in the z direction is defined as

$$w_0 = \begin{cases} w_0^d + w_0^p & 0 < t \le t_1 \\ w_0^d & t > t_1 \end{cases} \tag{4}$$

where t_1 is the total time of an impact excitation.

The stress-strain relationship at the k-th layer of the VC-FML plate is stated as

$$\begin{Bmatrix} \sigma_1 \\ \sigma_2 \\ \sigma_4 \\ \sigma_5 \\ \sigma_6 \end{Bmatrix}^{(k)} = \begin{bmatrix} Q_{11} & Q_{12} & & & \\ Q_{12} & Q_{22} & & & \\ & & Q_{44} & & \\ & & & Q_{55} & \\ & & & & Q_{66} \end{bmatrix}^{(k)} \begin{Bmatrix} \varepsilon_1 \\ \varepsilon_2 \\ \varepsilon_4 \\ \varepsilon_5 \\ \varepsilon_6 \end{Bmatrix} + \begin{Bmatrix} \bar{\sigma}_1 \\ \bar{\sigma}_2 \\ \bar{\sigma}_4 \\ \bar{\sigma}_5 \\ \bar{\sigma}_6 \end{Bmatrix}^{(k)} \tag{5}$$

where σ_1 and σ_2 are the normal stresses along the *x* and *y* directions, and σ_4, σ_5, σ_6 are the shear stresses in the *yz, xz, xy* planes, respectively, and ε_i are the corresponding strains. Besides, $Q_{ij}^{(k)}$ is the stiffness coefficient at the *k*-th layer. For the composite layer, $Q_{ij}^{(k)}$ is expressed as follows

$$Q_{11}^{(k)} = E_1 / 1-\upsilon_{12}\upsilon_{21}, Q_{12}^{(k)} = Q_{21}^{(k)} = \upsilon_{12}E_2 / 1-\upsilon_{12}\upsilon_{21}, Q_{22}^{(k)} = E_2 / 1-\upsilon_{12}\upsilon_{21}, Q_{44}^{(k)} = G_{23}, Q_{55}^{(k)} = G_{13}, Q_{66}^{(k)} = G_{12} \tag{6}$$

where E_1 and E_2 represent the Young's moduli parallel and perpendicular to the fibers, respectively, G_{12}, G_{13} and G_{23} represent the shear moduli in 1-2, 1-3 and 2-3 planes, respectively, and υ_{12}, υ_{21} are the corresponding Poisson's ratios.

For metal layers and the viscoelastic layer, $Q_{ij}^{(k)}$ has the following expressions

$$Q_{11}^{(k)} = E_\mu / 1-\upsilon_\mu^2, Q_{12}^{(k)} = Q_{21}^{(k)} = \upsilon_\mu E_\mu / 1-\upsilon_\mu^2, Q_{22}^{(k)} = E_\mu / 1-\upsilon_\mu^2, Q_{44}^{(k)} = Q_{55}^{(k)} = Q_{66}^{(k)} = E_\mu / 2(1-\upsilon_\mu) \ \ (\mu = \mathrm{M, V}) \tag{7}$$

where E_M, and υ_M are Young's moduli and Poisson's ratio of metal layers, and E_V, and υ_V are the counterparts of the viscoelastic layer.

Specifically, the corresponding residual stresses $\bar{\sigma}_i$ can be written as follows

$$\bar{\sigma}_i = \sigma_i^f Q_{ii}^{(k)} h_k / K_i h \tag{8}$$

where σ_i^f is the stress of a failure layer, h_k is the thickness of the *k*-th layer, and K_i is the equivalent stiffness of the overall structure, with the following expressions

$$K_1 = \frac{\bar{E}_1}{1-\bar{v}_{12}^2 \frac{\bar{E}_2}{\bar{E}_1}}, K_2 = K_1 \frac{\bar{E}_2}{\bar{E}_1}, K_4 = \bar{G}_{23}, K_5 = \bar{G}_{13}, K_6 = \bar{G}_{12} \tag{9}$$

where $\bar{E}_1$, $\bar{E}_2$, $\bar{G}_{23}$, $\bar{G}_{13}$, $\bar{G}_{12}$ and $\bar{v}_{12}$ are the equivalent moduli and Poisson's ratio, respectively, with the detailed expressions being given by

$$\bar{E}_1 = \frac{A_{11} - \frac{A_{12}^2}{A_{22}}}{h}, \ \bar{E}_2 = \bar{E}_1 \frac{A_{22}}{A_{11}}, \ \bar{G}_{23} = \frac{A_{44}}{h}, \ \bar{G}_{13} = \frac{A_{55}}{h}, \ \bar{G}_{12} = \frac{A_{66}}{h}, \ \bar{v}_{12} = \frac{A_{12}}{A_{22}} \tag{10}$$

where A_{ij} are the tensile stiffness coefficients.

2.3 Damage criterion based on critical impact velocity

According to the energy balance, when the impactor contacts with the VC-FML plate, the impact velocity V_0 can be written as

$$V_0 = \sqrt{\frac{2(U^p + T_d + T_f)}{M}} \tag{11}$$

where U^p, T_d and T_f are the strain energy generated by impact, the consumed energies in the delamination and tensile fracture, respectively.

After the impactor contacts the front face of the VC-FML plate, V_0^* is defined as the critical impact velocity (CIV) when the structural damage occurs with the following expression

$$V_0^* = \sqrt{\frac{2U^p}{M}} = \sqrt{\frac{2K_A(w_{\max}^*)^4 + K_B(w_{\max}^*)^3 + K_D(w_{\max}^*)^2}{M}} \tag{12}$$

where $w_{\max}^*$ is the maximum displacement at the impact center accounting for the possible damage in different layers. K_A, K_B, K_D are the tensile stiffness, tensile flexural coupling stiffness and flexural stiffness component, respectively, with the detailed expressions being given by

$$\begin{aligned}
K_A &= \frac{(2(R_2 - R_1))^{14}}{(\pi R_2^2)^8}\left[\frac{32}{45}(A_{11} + A_{22}) + 2(A_{12} + 2A_{66}) + \frac{8}{3}(A_{16} + A_{26})\right] \\
K_B &= -\frac{(2(R_2 - R_1))^{10}}{(\pi R_2^2)^6}\left[\frac{32}{21}(B_{11} + B_{22}) + \frac{128}{25}(B_{12} + 4B_{66}) + 16(B_{16} + B_{26})\right] \\
K_D &= -\frac{(2(R_2 - R_1))^{6}}{(\pi R_2^2)^4}\left[\frac{32}{5}(D_{11} + D_{22}) + \frac{64}{9}(D_{12} + 8D_{66}) + 32(D_{16} + D_{26})\right]
\end{aligned} \tag{13}$$

where $B_{ij,}$ D_{ij} are the corresponding stiffness coefficients, respectively.

The Von Mises equivalent stress criterion [37] for the metal layers is

$$\frac{\sigma_1^2 + \sigma_2^2 - \sigma_1\sigma_2 + 3\sigma_6^2}{\sigma_{\mathrm{M}}^e} = 1 \tag{14}$$

where σ_{M}^e is the equivalent yield stress of the metal layer, whose magnitude is the yield tensile strength of the metal layer when the low-velocity impact is taken into account.

The simplified Tsai-Hill criterion for the fiber layers is stated as [38]

$$\left(\frac{\sigma_1}{X_T}\right)^2 + \left(\frac{\sigma_2}{Y_T}\right)^2 - \frac{\sigma_1\sigma_2}{{X_T}^2} + \left(\frac{\sigma_6}{S_{\mathrm{f}}}\right)^2 = 1 \tag{15}$$

where X_T, Y_T and S_{f} are the longitudinal and the transverse tensile strengths and the shear strength of fiber reinforced material.

The Drucker-Prager stress failure criterion for the viscoelastic layer is expressed as [39]

$$\frac{\left[(\sigma_1-\sigma_2)^2+(\sigma_1-\sigma_6)^2+(\sigma_2-\sigma_6)^2\right]}{2\left[3(\sigma_{\rm v}^s)^2/(\sigma_{\rm v}^T)^2\left(\sigma_{\rm v}^T\right)^2-\left(3(\sigma_{\rm v}^s)^2/(\sigma_{\rm v}^T)^2-1\right)\sigma_{\rm v}^T(\sigma_1+\sigma_2+\sigma_6)\right]}=1 \quad (16)$$

where $\sigma_{\rm v}^T$ is the yield tensile strength of the viscoelastic layer, and $\sigma_{\rm v}^s$ is the yield shear strength.

By adopting the failure criteria described above for different material layers of the VC-FML plate, Fig. 2 illustrates a flow chart of the iterative computational approach to determine the maximum displacement $w_{\max}^*$. Firstly, set the initial value $w_{\max}^0=0$, and asaume that e_0 and c represnt the initial step size and precision coefficient, and $e=e_0/2^{j_a}$ denotes the step size, in which j_a is the number of failures in the iteration process. After the iterative calcuations start, substitute $w_{\max}^i$ calculated in the i step into Eqs. (2)-(5) to obtain $\sigma_1,\sigma_2,\sigma_6$. Subsequently, bring stress results into Eqs. (14)-(16) to estimate whether structural damage happens. If the failure criteria are less than 1, there is no damage occurred in the structure, followed by letting $w_{\max}^{i+1}=w_{\max}^i+e$. Otherwise, update e to reduce this value to a half of the previous one. At the meantime, let $w_{\max}^{i+1}=w_{\max}^{i-1}+e$. By repeating the above interative calcuations untill $e<c$, the final interative value of $w_{\max}^i$ is obtained that can be regarded as $w_{\max}^*$.

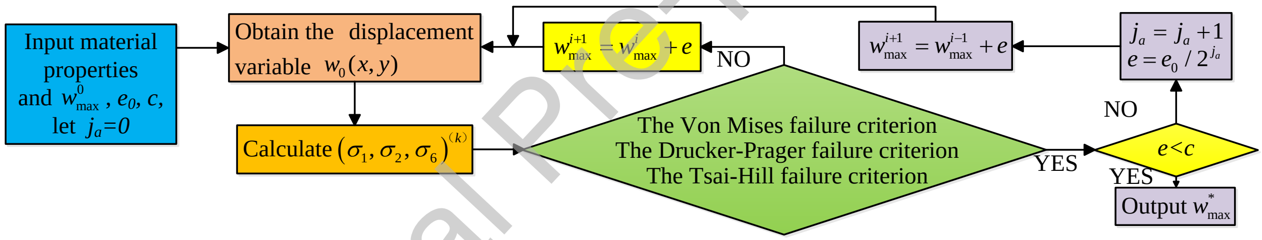

Fig. 2. A flow chart of iterative computations for determining $w_{\max}^*$.

Furthermore, to construct a critical impact velocity criterion, J_A is defined as a critical impact velocity ratio with the following expression

$$J_A=\frac{V_0^2M}{2K_A(w_{\max}^*)^4+K_B(w_{\max}^*)^3+K_D(w_{\max}^*)^2}\le 1 \quad (17)$$

By adopting the predefined criterion described in Eq. (17), one can quantitatively estimate whether the VC-FML plate is damaged or not. Bring different V_0 into this equation to obtain the corresponding critical impact velocity ratio J_A, if J_A meet the reqiurement in Eq. (17), it can be assumed that there is no damage occoured in the VC-FML plate. At this time, it is only needed to solve the free and forced vibrations (further description on this will be given in Section 2.4). Otherwise, the structural damage due to impact load has to be taken into account. Thus, it is necessary to solve the dynamic response with coupling vibration and impact of the VC-FML structure (further discussion to be given in Section 2.5).

2.4 Solution of free and forced vibrations without considering impact damage

If the impact damage does not occur in the VC-FML plate, the resulting deformation remains in an elastic range. Therefore, only free and forced vibrations need to be considered. At this elastically contacted state between the impactor and the target, the total potential energy U_s with impact excitation is expressed as

$$U_s = U^p - Fw_{\max} \tag{18}$$

When $\partial U_s / \partial w_{\max} = 0$, U_s will reach the maximum value. At this time, the maximum impact contact force $F_{\max}$ is given by

$$F_{\max} = \partial U^p / \partial w_{\max} \tag{19}$$

Suppose that the impact excitation load $F(x, y, t)$ is expressed as below

$$F(x,y,t) == \begin{cases} F_{\max} \sin(\pi t / t_1)\delta(x - x_1)\delta(y - y_1), & 0 \le t \le t_1 \\ 0 & , \quad t > t_1 \end{cases} \tag{20}$$

where $\delta(x - x_1)\delta(y - y_1)$ is the Dirac delta function.

Since the impact velocity does not reach to V_0^*, t_1 can be written as follows

$$t_1 = \frac{2MV - 2M\sqrt{V^2 - 2F_{\max} w_{\max} / M}}{F_{\max}} \tag{21}$$

Thus, the total strain energy U and kinetic energy T of the VC-FML plate are obtained as

$$U = U_{\mathrm{M}} + U_{\mathrm{F}} + U_{\mathrm{V}} \tag{22a}$$

$$T = T_{\mathrm{M}} + T_{\mathrm{F}} + T_{\mathrm{V}} \tag{22b}$$

where $U_{\mathrm{M}}, U_{\mathrm{F}}, U_{\mathrm{V}}$ are the strain energies of metal layers, fiber layers and viscoelastic layer, respectively, and $T_{\mathrm{M}}, T_{\mathrm{F}}, T_{\mathrm{V}}$ are the corresponding kinetic energies. Their detailed expressions are provided in the Appendix.

The Lagrange function L is obtained as

$$L = T - U \tag{23}$$

By minimizing L with respect to A_{mn} B_{mn} C_{mn} D_{mn} E_{mn}, the following expressions are obtained.

$$\frac{\partial L}{\partial A_{mn}} = \frac{\partial L}{\partial B_{mn}} = \frac{\partial L}{\partial C_{mn}} = \frac{\partial L}{\partial D_{mn}} = \frac{\partial L}{\partial E_{mn}} = 0 \tag{24}$$

Thus, the equation of motion of the overall structure system is expressed as

$$\left(\boldsymbol{K} + \mathrm{i}\boldsymbol{C} - \omega^2 \boldsymbol{M}\right)\boldsymbol{q} = \boldsymbol{F} \tag{25}$$

where $\boldsymbol{K}$, $\boldsymbol{M}$ and $\boldsymbol{C}$ are the stiffness, mass and damping matrices with the expressions as follows

$$\boldsymbol{K}=\mathrm{diag}\left(\frac{\partial U}{\partial A_{mn}},\ \frac{\partial U}{\partial B_{mn}},\ \frac{\partial U}{\partial C_{mn}},\ \frac{\partial U}{\partial D_{mn}},\ \frac{\partial U}{\partial E_{mn}}\right) \tag{26a}$$

$$\boldsymbol{M}=\mathrm{diag}\left(\frac{\partial T}{\partial A_{mn}},\ \frac{\partial T}{\partial B_{mn}},\ \frac{\partial T}{\partial C_{mn}},\ \frac{\partial T}{\partial D_{mn}},\ \frac{\partial T}{\partial E_{mn}}\right)/\,\omega^2 \tag{26b}$$

$$\boldsymbol{C}=\beta\boldsymbol{M}+\gamma\boldsymbol{K} \tag{26c}$$

where β and γ are the proportional damping coefficients related to the stiffness and mass matrices.

By ignoring $\boldsymbol{C}$ and $\boldsymbol{F}$ in Eq. (25), the free vibration equation is given by

$$\left(\boldsymbol{K}-\omega^2\boldsymbol{M}\right)\boldsymbol{q}=0 \tag{27}$$

where $\boldsymbol{q}$=[A_{mn} B_{mn} C_{mn} D_{mn} E_{mn}]$^{\mathrm{T}}$ is the eigenvector, To solve the angular natural frequencies, Eq. (27) should has a nonzero or nontrivial solution. Thus, ω and $\boldsymbol{q}$ can be obtained. Moreover, by substituting $\boldsymbol{q}$ into Eq. (2), each modal shape can also be solved.

To study the vibration response of the VC-FML plate, the following expression is assumed

$$X(t)=\sum_{m=1}^{\infty}\sum_{n=1}^{\infty}W_{mn}(x,y)T_{mn}(t) \tag{28}$$

where $W_{mn}(x,y)$ is the modal shape; $T_{mn}(t)$ represents the shape component. Based on the Duhamel integral principle, the detailed expression of $T_{mn}(t)$ is given by

$$T_{mn}(t)=\frac{W_{mn}\left(x_1,y_1\right)}{\omega_r\sqrt{1-\zeta_r^2}\int_A\rho h\left(W_{mn}(x,y)\right)^2\mathrm{d}A}\int_0^t\frac{F(\tau)}{\delta(x-x_1)\delta(y-y_1)}\mathrm{e}^{-\zeta_r\omega_r\sqrt{1-\zeta_r^2}(t-\tau)}\sin[\omega_r\sqrt{1-\zeta_r^2}(t-\tau)]\mathrm{d}\tau \tag{29}$$

where ρ is the density; ω_r is the r-th natural frequency; ζ_r is the r-th modal damping ratio obtained through experimental tests, which is also utilized to determine β and γ with the expression of $2\zeta_r\omega_r=\beta+\gamma\omega_r^2$.

Finally, by substituting the calculated results from Eq. (29) into Eq. (28), the time-domain vibration response of this type of composite structures subjected to impact excitation load can be solved.

2.5 Solutions of impact and vibration characteristics considering impact damage

If the impact damage already occurs in the VC-FML plate structure, both impact and vibration parameters at this state need to be solved. Firstly, by applying the progressive quasi-static approach, the failure event [20] is introduced to establish the bending stiffness coefficient $\bar{D}_{ij}^q(x,y)$ at the impact position, whose expression related to the q-th failure event, is defined as [40]

$$\bar{D}_{ij}^q(x,y)=D_{ij}^{q-1}\left[1-\delta_q\psi_{ij}^q\gamma_d(x,y)\right]\qquad(i,j=1,2,4,5,6) \tag{30}$$

where δ_q is a factor to describe the degree of damage in the q-th failure events; ψ_{ij}^q is a factor to describe the direction of damage; $\gamma_d(x, y)$ is the damage geometry parameter with the following expression

$$\gamma_d(x, y) = \frac{9K_1T_0}{8\pi\left(h\tau_a\right)^2}\delta(x - x_1)(y - y_1) \tag{31}$$

In the calculations, the values of δ_q and ψ_{ij}^q related to the *q*-th failure event are predefined, as shown in Table B1 in Appendix B.

The impact contact force F_q at the *q*-th failure event in the VC-FML plate is expressed as

$$F_q = \partial U_q^p / \partial w_{\max} \tag{32}$$

Thus, the total strain energy U_q absorbed by the overall structural system is given by

$$U_q = U_q^p - U_{q-1}^p \tag{33}$$

where U_q^p and U_{q-1}^p are the strain energies related to the *q*-th and *q*-1th failure events.

The contact radius R_1^q in the *q*-th failure event is defined as follows

$$R_1^q = \sqrt{w_{\max}^q(2R - w_{\max}^q)} \tag{34}$$

where R is the radius of hemispherical head of impactor.

The absorbed energy T_d^q at the *q*-th failure event in the VC-FML plate is written as

$$T_d^q = \frac{\pi\bar{E}_1^q hG_{II}^2}{9\left(1-(\bar{v}_{12}^q)^2\right)\left(\sigma_{IL}\right)^2} + \frac{\pi\bar{E}_2^q hG_{II}^2}{9\left(1-(\bar{v}_{21}^q)^2\right)\left(\sigma_{IL}\right)^2} \tag{35}$$

where G_{II} is the mode II critical inter-laminar energy release rate of the adhesive caused by the delamination [41]. σ_{IL} is the inter-laminar shear strength, $\bar{E}_1^q$,$\bar{E}_2^q$ are the equivalent elastic moduli in different fiber directions of the VC-FML plate when the *q*-th failure event occurs, and $\bar{v}_{12}^q$, $\bar{v}_{21}^q$ are the equivalent Poisson's ratios. It is worth noting that since the metal layers and the viscoelastic layer are made of isotropic materials, fiber directions of "1" and "2" are taken as the main ones to improve the computing efficiency.

Furthermore, the tensile fracture energy T_f^q in the *q*-th failure event is written as

$$T_f^q = w_{\max}^q \pi e_t R_q^2 / 3 \tag{36}$$

where e_t is the energy density of the failure layer, which is closely related to the yield tensile strength and ultimate tensile strength in the layer studied.

Thus, the total consumed energy T_a^q corresponding to the *q*-th failure event is expressed as

$$T_a^q = U_q + T_d^q + T_f^q \tag{37}$$

The impact velocity V_q when the *q*-th failure event happens is stated as

$$V_q = \sqrt{\left(MV_{q-1}^2 - 2T_a^{q-1} / M\right)} \tag{38}$$

Finally, impact time t_q in the light of the *q*-th failure event is determined as follows

$$t_q = \frac{\left[M + \pi(R_1^q)^2\rho_a + \frac{1}{9}(a-2R_1^q)(b-2R_1^q)\rho_a\right]\left|V_q - V_{q-1}\right| + C_s^q(w_{\max}^q - w_{\max}^{q-1})}{F_q - K_s^q w_{\max}^q} + t_{q-1} \tag{39}$$

where ρ_a is surface density; K_s^q and C_s^q are overall shear stiffness and viscous damping coefficients, respectively; V_{q-1}, V_q, $w_{\max}^{q-1}$, $w_{\max}^q$ and t_q, t_{q-1} represent the corresponding velocities, the maximum displacements and the time at the impact center in the *q*-1th and *q*-th failure events, respectively.

In this way, the impact contact force F_q, the displacement $w_{\max}^q$ and the time t_q corresponding to each failure event *q* are all obtained, which are essential for plotting the concerned load-displacement curves. Meanwhile, to solve the vibration behavior accounting for damage effect, the total failure event $\bar{q}$ is defined in the impact process. Due to that $t > t_{\bar{q}}$, $\bar{D}_{ij}^{\bar{q}}$ in Eq. (30) is substituted into Eq. (22) to solve the strain energy U and kinetic energy T of the VC-FML plate. Hence, each natural frequency ω and modal shape $W_{mn}(x,y)$ related to impact damage can be solved by Eqs. (23)-(27). Finally, let $t_1 = t_{\bar{q}}$ and also bring the maximum contact force $F_{\max} = \max(F_q)$ into Eq. (20), and then employ Eq. (29) combined with $W_{mn}(x,y)$ to solve the shape component $T_{mn}(t)$. On the basis of those results, the vibration response considering impact damage can be solved.

2.6 Numerical validation

Firstly, the numerical results from Ref. [29] are utilized to verify the model developed in prediction of impact responses. Three identical sandwich plates with the viscoelastic core and the surface-layer configuration of $[0_2^\circ / 90_2^\circ / 0_2^\circ / \mathrm{core} / 0_2^\circ / 90_2^\circ / 0_2^\circ]$ are taken as the calculation examples. The theoretical results are obtained based on the model developed at three different impact points by ignoring the effect of metal layers. The following geometrical and material parameters are chosen in the calculations, i.e. E_1=E_2=54 GPa, G_{12}=3.16 GPa, G_{13}=G_{23}=1.87 GPa, υ_{12}=0.313, ρ_{f}=1511 $\mathrm{kg/m^3}$, h_{f}=1.584 mm, E_{v}=0.18 GPa, υ_{V}=0.286, ρ_{V}=110 $\mathrm{kg/m^3}$, h_{v}=12.7 mm, and *a*=*b*=76.2 mm. Meanwhile, the radius, mass and initial velocity of the impactor are 12.7 mm, 1.8 kg, and 3.7 m/s, respectively. Table 1 lists the comparisons of the maximum impact displacements, contact forces and absorbed energies of those sandwich plates between the present study and the Ref. [29]. It is clear that the relative deviations of the maximum displacement, contact force and absorbed energy are only 3.5, 3.0 and 3.8 %, respectively, which are within an acceptable range. Moreover, Fig. 3 presents the comparison of the impact contact force-time history and the displacement-time history curves, with the impact point located at $x_1=y_1=3a/4$, which also show a good agreement. The minor deviation may be attributed to neglecting the effects of the continuity of interlaminar stress in the present model.

Table 1. Comparison of the key parameters of three sandwich plates with viscoelastic cores between the present study and the Ref. [29] with different impact points.

Impact point	Max. contact force			Max. displacement			Absorbed energy		
	Ref. [29] /kN	The present /kN	Deviation /%	Ref. [29] /mm	The present /mm	Deviation /%	Ref.[29] /J	The present /J	Deviation /%
$x_1=a/2$, $y_1=a/2$	5.373	5.490	2.1	3.92	3.99	2.7	5.20	5.32	2.3
$x_1=3a/4$, $y_1=a/2$	5.476	5.596	2.1	3.71	3.82	2.9	5.62	5.73	1.9
$x_1=3a/4$, $y_1=3a/4$	5.608	5.783	3.0	3.60	3.67	3.5	6.02	6.26	3.8

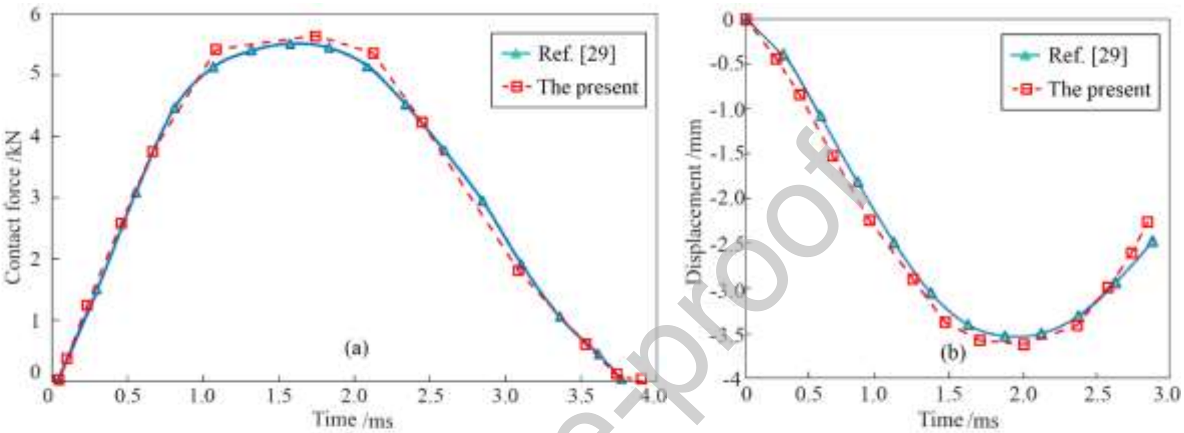

Fig. 3. Comparison of the time-history curves of (a) impact contact force and (b) displacement response between the present study and Ref. [29].

Furthermore, results from Ref. [33] are employed to validate the validity of the model developed in predicting free vibration results of the composite plate structure. A rectangular sandwich plate comprised of two anisotropic fiber layers and one viscoelastic core with four-edged-fixed boundary conditions is taken as a calculation example. The material parameters are already provided in Ref. [33]. In the calculations, the corresponding non-dimensional frequency results are obtained by the present model with ignoring the effect of metal layers. Table 2 shows the comparisons of the non-dimensional natural frequencies in the first four modes between the present study and the Ref. [33]. It can be seen that the deviations of those frequency parameters are less than 1 %, which shows a good agreement again, since the Rayleigh-Ritz method is adopted by both studies with the same truncation coefficients being selected.

Table 2. Comparison of the first four non-dimensional natural frequencies of the sandwich plate with a viscoelastic core between the present study and the Ref. [33].

Category	Modal order			
	1	2	3	4
Present study	2.131	3.745	3.745	5.371
Ref. [33]	2.130	3.740	3.742	5.365
Relative deviation /%	0.06	0. 19	0.08	0.11

3 Experimental validation

3.1 Experimental setup

Here, four 5-layer VC-FML plate specimens, namely specimens I to IV, with identical material and geometrical parameters, are measured. Each specimen includes two metal layers, two fiber layers and one viscoelastic core. The metal is titanium alloy (Yuanli Xin Materials Co. Ltd in China), fiber material is TC300 carbon fiber/ FRD-YG-03 resin with the configuration of $[0^\circ/90^\circ/0^\circ/90^\circ]$ (Jiujiang Diwei Composite Material Co., Ltd. in China), and viscoelastic material is ZN-33 rubber (Beijing Xingdaxin Special Materials Co., Ltd. in China). To ensure a good repeatability of experimental results, the four-edge-fixed boundary condition is chosen for the plate specimens that is constrained by a set of clamping fixture with M8 bolts, since it is much easier to simulate than the four-edge-simply-supported boundary condition. The effective length, width and thickness of those specimens after the clamping are 170, 160 and 2.6 mm, respectively. Besides, the material properties and thickness of each layer are shown in Table 3.

Table 3. Material properties and thickness of each layer in the VC-FML plate specimens.

Type	Elastic moduli /GPa					Density /kg/m^3	Poisson's ratio	Thickness /mm	Ultimate strength /GPa		
	E_1, E_v, E_m	E_2	G_{12}	G_{13}	G_{23}				$\sigma_M^e, X_T, \sigma_V^T$	Y_T	S_f
Fiber layer	136	7.9	4.0	4.5	5	1780	0.30	0.5	2.21	0.049	0.135
Viscoelastic layer	0.005	--	--	--	--	930	0.49	1	0.007	--	--
Metal layer	108	--	--	--	--	4150	0.30	0.3	0.6	--	--

An integrated testing system of the VC-FML plate specimens for impact and vibration experiment is shown in Fig. 4, which consists of three subsystems, namely the impact excitation, vibration excitation, and measuring and recording ones. The first subsystem involves an impactor (with total mass of 1 kg), a guide cylinder with a complete scale icon and an impactor-release device, with the similar design and excitation methodology utilized in Ref. [42-43]. The head of the impactor is designed as a "hemispherical" shape with a diameter of 8.0 mm. The height can be determined via the scale value marked in the guide cylinder ranged from 0 to 1200 mm. Thus, the impact velocity can be indirectly obtained with the kinetic energy formula of $mgH = 0.5mV^2$. The second subsystem includes a PCB 086C01 modal hammer that can provide a pulse excitation to the specimens tested. The third subsystem consists of a contacting displacement sensor (model: LSM2-10), a dynamic force sensor (model: Sinocera CL-YD-305), a laser Doppler vibrometer (model: PDV-100), a LMS SCADAS data acquisition instrument and a Notebook PC. In the measuring process, the dynamic force sensor and the displacement sensor are employed to obtain the impact contact force and response signals, and the laser vibrometer is used to obtain the vibration response signal. All of the force, displacement and vibration response signals are recorded with the help of the LMS Test Lab.10b software installed in the Notebook PC. In addition, the following parameters are chosen in the dynamic experiment: (1) sample frequency for impact measurement: 20480 Hz; (2) sample frequency for vibration measurement: 4096 Hz; (3) frequency resolution for impact measurement: 0.3 Hz; (4)

frequency resolution for vibration measurement: 0.1 Hz; (5) impact velocity range: 0.98-4.82 m/s; (VI) pulse excitation range for vibration measurement: 0.025-0.035 kN.

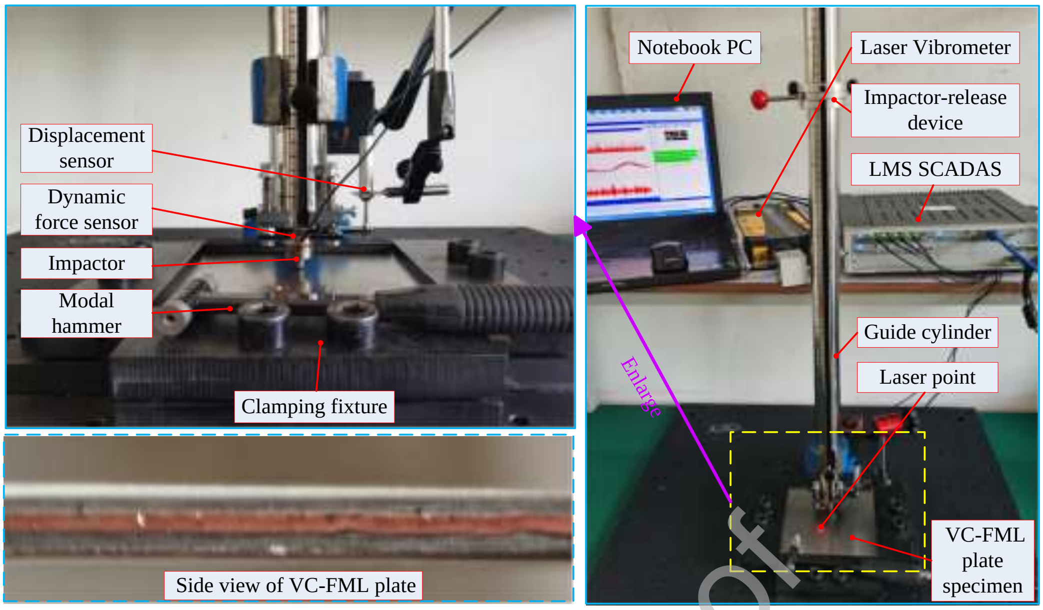

Fig. 4. An integrated testing system of the VC-FML plate specimens for the coupled impact and vibration experiment.

3.2 Comparison of theoretical and experimental results

Before conduct the impact test, the first three natural frequencies of each plate specimen are measured by hammer excitation technique, with results being listed in Table 4. Then, four impact heights are applied to the specimens I to IV, i.e. 300, 600, 1000 and 1200 mm, corresponding to impact velocities of 2.42, 3.43, 4.43 and 4.82 m/s, respectively. Note that the first impact velocity is less than the CIV of 2.55 m/s (which can be determined based on the iterative method shown in Fig. 2 together with Eq. (12)), whereas the last three ones are all higher than the CIV. The photographs of those specimens after the impact test are given in Fig. 5, in which a progressively aggravated indentation can be observed on the surface of the VC-FML plate specimens. Meanwhile, the natural frequencies of each plate specimen after the impact test are measured again, with consideration of the deformation or possible damage, which are also listed in Table 4 for the detailed comparison. It can be observed from Fig. 5 and Table 4 that, when the impact velocity is higher than 3.43 m/s, more clear indentations appear on the surfaces of specimens II to IV, followed by a more noticeable reduction of the first three natural frequencies with the maximum reduction of 27.3 % (Table 4). Thus, the plastic damage occurs in those three specimens. However, when the impact velocity is 2.42 m/s, the surface of specimen I has no impact damage, as the corresponding natural frequency results remain unchanged before and after the impact test. Therefore, it is reasonable to believe that the predicted CIV result is indirectly validated.

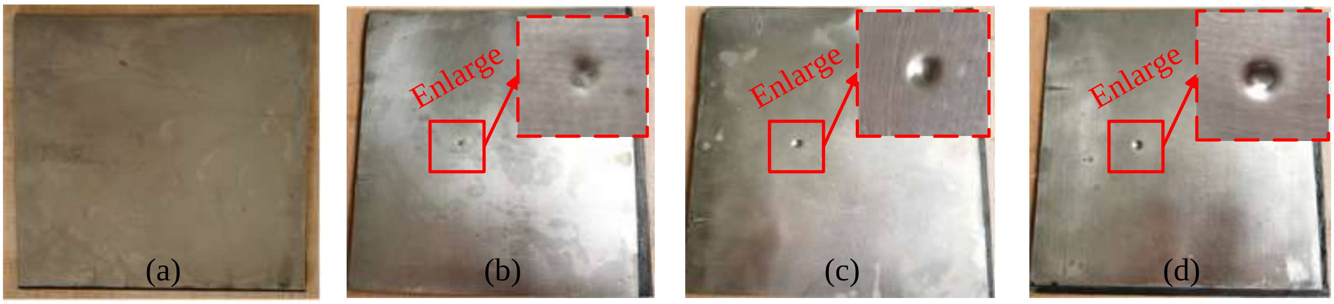

Fig. 5. Photographs of the VC-FML plates tested: (a) specimen I, (b) specimen II, (c) specimen III and (d) specimen IV.

Table 4. Comparison of the experimental natural frequencies of four different plate specimens in the first three modes.

Type	Specimen I			Specimen II			Specimen III			Specimen IV		
	First mode	Second mode	Third mode	First mode	Second mode	Third mode	First mode	Second mode	Third mode	First mode	Second mode	Third mode
Before impact test /Hz	388.5	750.9	837.5	388.6	747.5	837.5	382.2	751.3	839.6	388.5	750	838.1
After impact test /Hz	388.5	750.9	837.5	350.2	593.8	736.3	317.5	551.3	708.8	310.5	545	686.3
Reduction (%)	0	0	0	-9.8	-20. 6	-12.1	-16.9	-26.6	-15.6	-20.1	-27.3	-18.1

Table 5 gives the measured impact maximum contact forces and displacement amplitudes of the specimens II to IV subjected to different impact velocities. For the detailed comparison, the calculated results based on the proposed model are also listed in the same table. Additionally, the relative calculation errors between the theoretical calculations and experimental tests are provided in Table 5 as well. Furthermore, Fig. 6 compares the theoretical and experimental curves of impact contact force – time history, impact displacement – time history and load – displacement of those specimens subjected to impact velocities of 3.43, 4.43 and 4.82 m/s, respectively. It can be seen from Table 5 and Fig. 6 that the calculation errors of the maximum impact contact force and the corresponding displacement are less than 6.8 % and 8.9 %, respectively. Along with the increment of impact velocity, the peak contact force in the load-displacement curve (Fig. 6c) exhibits a significant uptrend with the maximum increase of 72.4 %. Also, the predicted curves agree well with the experimental ones in the impact velocity range studied. Hence, the model developed has provided a good prediction on the impact responses of VC-FML plates. The calculation errors are probably due to that in the integrated model the impact area is regarded as an ideal circle, but it is mostly elliptic in fact. Another reason is that the Tsai-Hill criterion adopted in this study has some limits on the damage failure modes, including fiber compression failure, matrix tensile and compression failure.

Table 5. Comparison of the maximum impact contact forces and displacement amplitudes of the specimens II to IV between the theoretical calculations and experimental tests subjected to different impact velocities.

Type	Specimen II		Specimen III		Specimen IV	
	F_{max} /kN	w_{max} /mm	F_{max} /kN	w_{max} /mm	F_{max} /kN	w_{max} /mm
Experimental	1.978	4.47	2.793	5.71	3.411	6.12
Theoretical	1.843	4.15	2.605	5.20	3.353	5.67
Calculation error/%	6.8	7.2	6.7	8.9	1.7	7.3

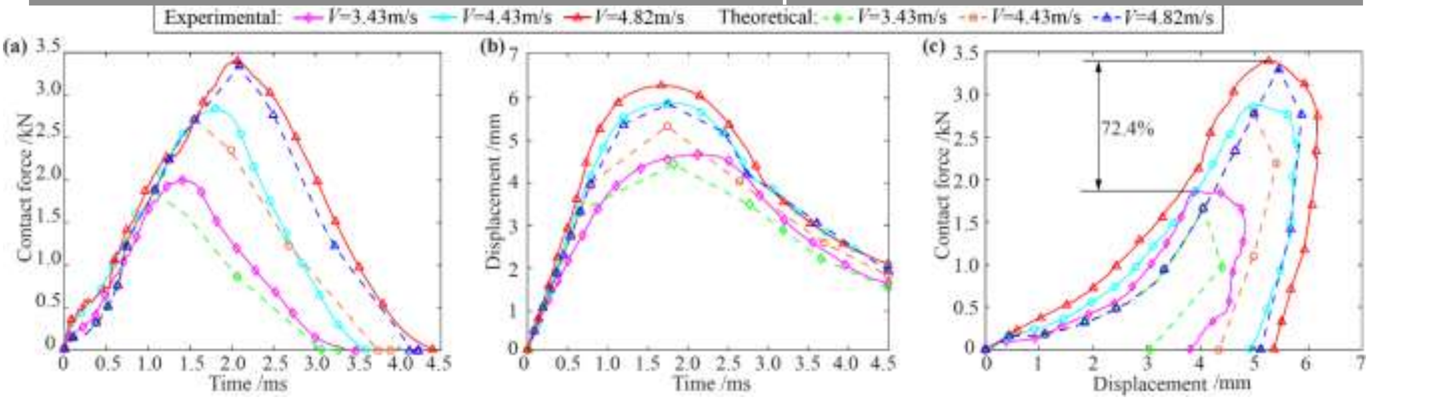

Fig. 6. Comparison of theoretical and experimental curves (a) impact contact force-time history, (b) displacement-time history and (c) load-displacement of the VC-FML plate specimens subjected to different impact velocities.

To investigate the changes of vibration characteristics of the VC-FML plate structures after the impact excitation, Fig. 7 presents the comparison of time-domain displacement responses of the specimens I to IV between the theoretical calculations and experimental measurements within the time range of 0-0.04 s with different impact velocities. The examination of the Fig. 7 shows that the predicted variation trends of displacement responses are consistent with the experimental ones, which give the further validation of the proposed integrated model.

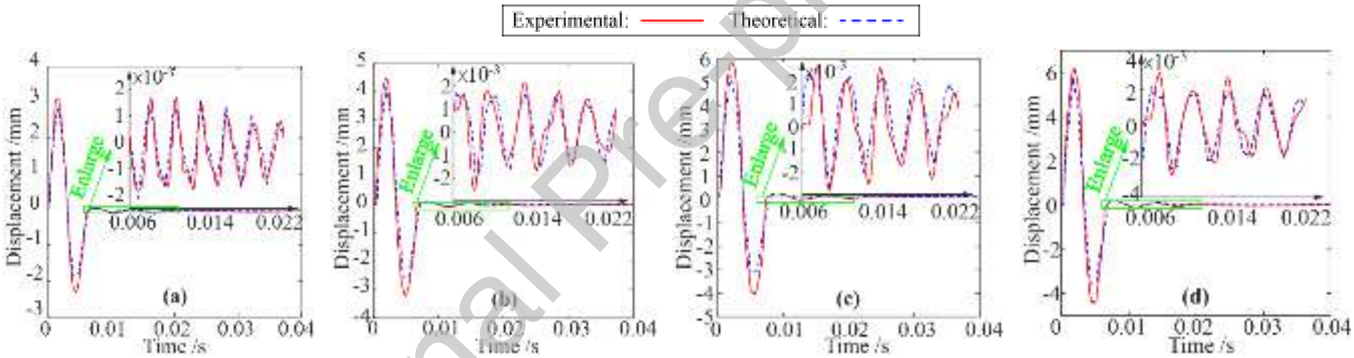

Fig. 7 Comparison of theoretical and experimental displacement responses of the VC-FML plate: (a) specimen I, (b) specimen II, (c) specimen III and (d) specimen IV within the time range of 0-0.04 subjected to different impact velocities.

Moreover, a variational mode decomposition (VMD) method [44] is adopted to decompose the response data within 0.006-0.022 s obtained in Fig. 7. Fig. 8 presents the comparison of the theoretical and experimental time-domain displacement responses in the first three modes of those specimens subjected to impact in different velocities. Then, conduct the fast Fourier transform (FFT) on those time data, the corresponding frequency-response curves are obtained, as shown in Fig. 9. It is clear that the discrepancy between the theoretical predictions and experimental results on natural frequencies and frequency-response amplitudes of the VC-FML plate specimens associated with the first three modes are less than 6.0 % and 9.8 %, respectively. The possible reasons for these errors are: (1) the damping variation affected by impact damage is not considered; (2) in the modeling, the relative slip effects between each layer are ignored.

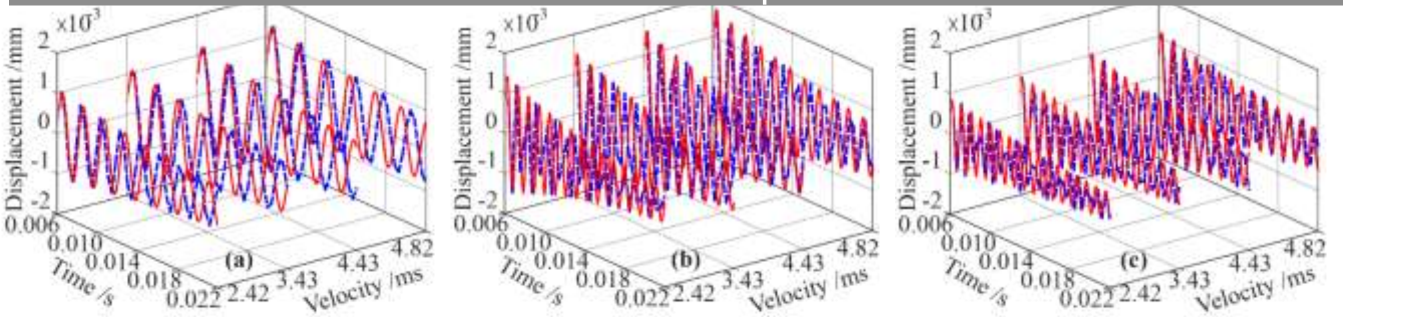

Fig. 8. Comparison of theoretical and experimental time-domain displacement responses in (a) the first mode, (b) the second mode and (c) the third mode of those specimens with different impact velocities obtained by the VMD method.

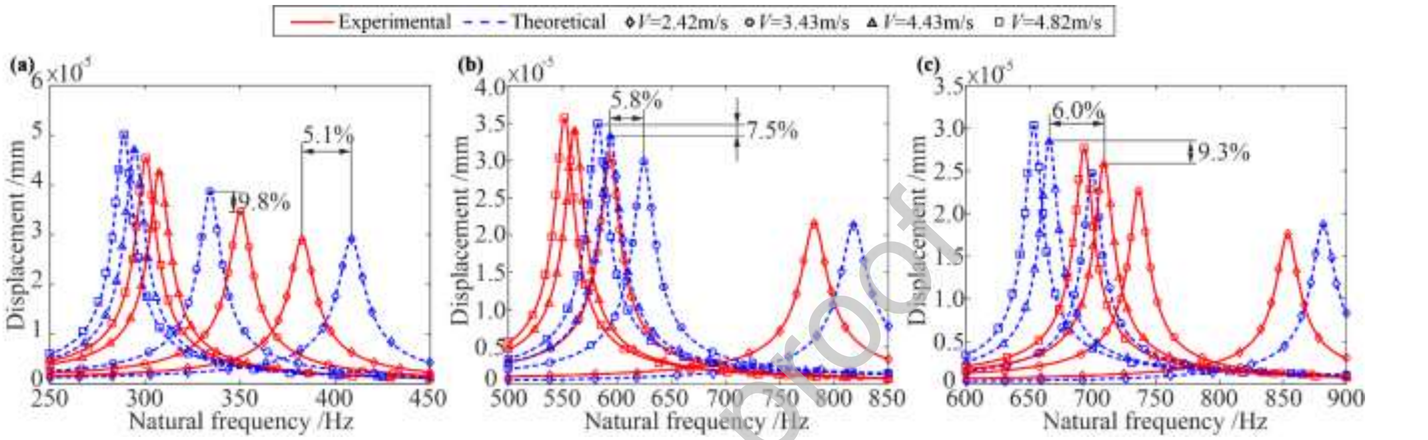

Fig. 9. Comparisons of theoretical and experimental frequency-response curves associated with (a) the first mode, (b) the second mode and (c) the third mode of those specimens with different impact velocities obtained by the VMD method.

To further clarify the variation trend of natural frequencies and displacement response perk of those specimens along with the increment of impact velocity, Fig. 10 displays the theoretical and experimental frequency and response results associated with the first three modes. It can be observed that as the impact velocity increases from 0 to 4.82 m/s, both the theoretical and the experimental natural frequency results remain unchanged when it is lower than the CIV. However, when it is higher than the CIV, with the increase of impact velocity, the structural natural frequencies exhibit a gradually declining trend due to the reduced stiffness by local indentation plastic deformations, whereas the displacement response perks show the uptrend. By taking the experimental results as examples, the maximum reduction of natural frequencies and the maximum rising degree of response perks reach 27.5 % and 61.2 %, respectively.

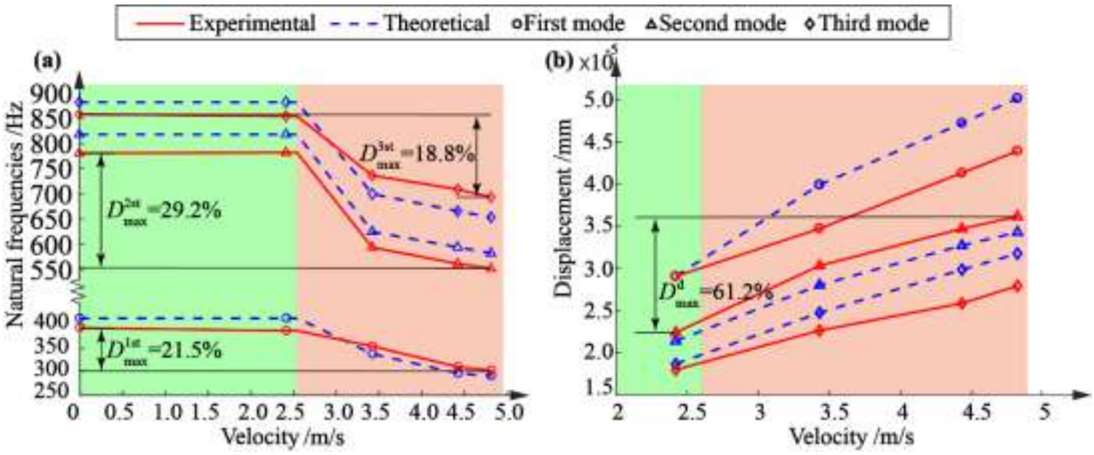

Fig. 10. The theoretical and experimental (a) natural frequencies and (b) displacement response perks of those specimens with different

impact velocities obtained by the VMD method.

4 Results and discussions

4.1 The effects of thickness ratio of viscoelastic layer to the VC-FML plate on impact and vibration responses

Based on the validated model, the effects of thickness ratio of viscoelastic layer to the VC-FML plate on the impact and vibration responses are investigated, which is shown in Fig. 11. In the calculations, the geometrical and material parameters of the VC-FML plate are listed in Table 3 with V=4.82 m/s. It is worth noting that: (1) the initial thickness ratio $T_h = h_v/h$ is set as 20 %; (2) the total thickness of VC-FML plate is unchanged, but the thicknesses of metal layers and fiber layers decrease proportionally with increasing the thickness of the viscoelastic layer. Here, the maximum relative variation rates of the contact force (namely D_{c}), natural frequencies (namely D_{f}) and displacement response perks (namely D_{d}) are marked in Figs. 11(a)-11(c). Note that in the following discussion, if there is no specific explanation, D_{c}, D_{f} and D_{d} associated with other influencing factors are all calculated and displayed in the corresponding figures.

It can be observed from Fig. 11(a) that, as the thickness ratio T_h increases from 20 to 70 %, the peak of contact force in load-displacement curves shows a downward trend with D_{c} = -46 %, which indicates that the impact resistance is reduced due to the weakened rigidity of the overall plate structure. Also, for the same reason, the normalized natural frequencies are decreased with D_{f} = -34.1 % (Fig. 11b). However, the vibration suppression effect is improved, since the displacement response perk is lowered obviously with D_{d} = -82.1 % (Fig. 11c). Hence, to ensure a good impact and vibration resistant performance, it is recommended that the thickness ratio of viscoelastic layer to the VC-FML plate needs to be selected within a range of 30-40 %. This is because the contact force peak is only reduced by about 15%, but the displacement response perk is decreased by more than 30 % in this range.

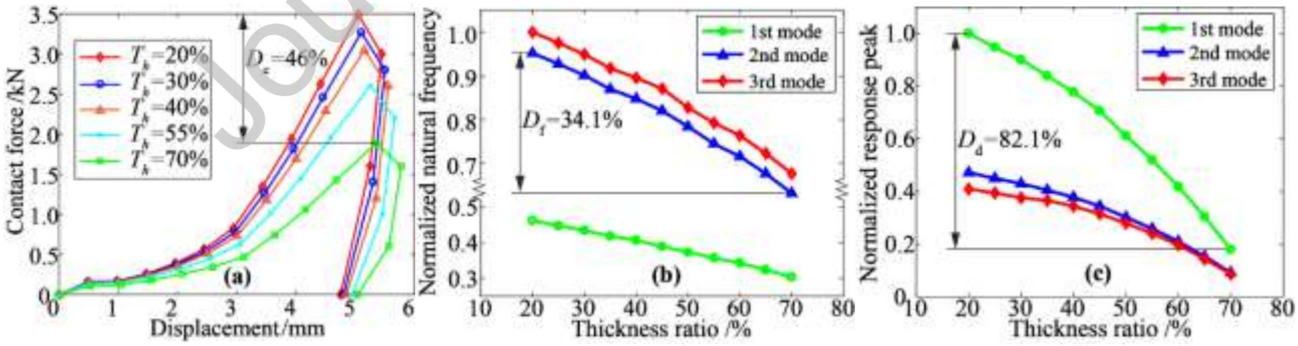

Fig. 11. Effects of thickness ratio of viscoelastic layer to the VC-FML plate on the impact and vibration responses: (a) load-displacement curves, (b) normalized natural frequencies and (c) normalized response perk.

4.2 The effects of the increase multiple of Young's moduli of viscoelastic layer to the VC-FML plate on impact and vibration responses

Fig. 12 presents the effects of the increase multiple of Young's moduli of viscoelastic layer E_{en} on the impact and vibration responses of the VC-FML plate, which are obtained with the impact velocity of 4.82 m/s and the same geometrical and material parameters provided in Table 3. It can be seen from Fig. 12 that as the Young's moduli of viscoelastic layer increases by 6 times, the contact force peaks in the load-displacement curve and vibration displacement response perks only increase slightly (Fig. 12a). Meanwhile, the relatively small variation of natural frequencies for all three modes can be observed (Fig. 12b). Therefore, to improve the vibration and impact resistance capabilities of the VC-FML plate, it is unwise to increase the elastic modulus of the viscoelastic layer, since this value is very small compared to the counterparts of other constituent layers.

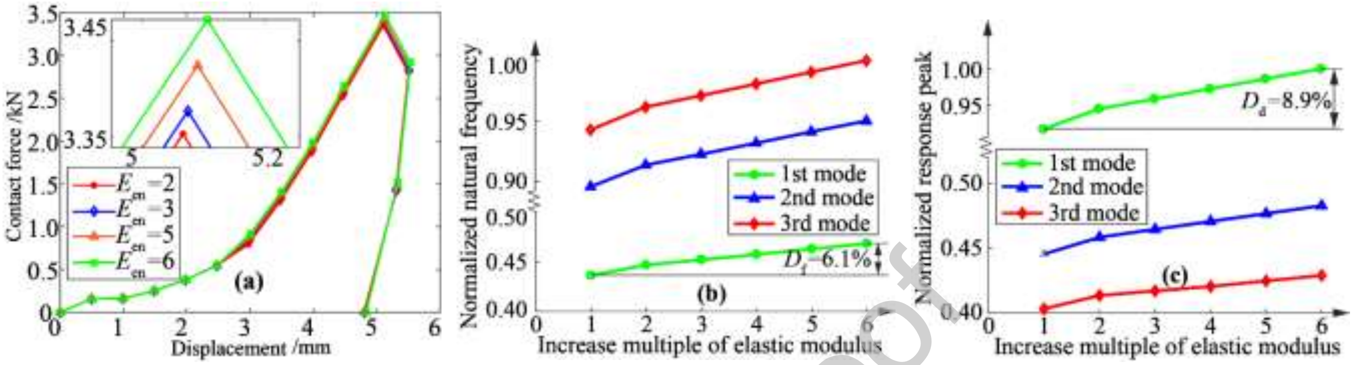

Fig. 12. The effect of Young's moduli of viscoelastic layer on the impact and vibration responses of the VC-FML plate: (a) load-displacement curves, (b) the normalized natural frequencies and (c) the normalized response perks.

5 Conclusions

In this study, a critical impact velocity criterion is proposed to couple the vibration and impact analyses of the hybrid fiber metal laminates with a viscoelastic layer. On the basis of this criterion, an integrated model is developed to predict two types of dynamic behaviors simultaneously. In this model, the impact point can be arbitrarily selected rather than the center point of the plate, which expands the scope of impact excitation. Since the effect of impact damage is considered, the prediction accuracy of vibration and impact parameters are improved. In addition, a series of numerical and experimental comparison are carried out to validate the model. Based on theoretical and experimental results, conclusions can be drawn as follows.

(1) When the low-velocity impact excitation exceeds the critical impact velocity (2.52 m/s) up to 4.82 m/s, the clear indentation appears on the surface of the composite plate specimen, followed by the further aggravated impact damage with the maximum increment on the contact force peak by 72.4 %. By taking the measured data as an example, the vibrational displacement response perks is continuously increased with the impact velocity, of which the corresponding rising degree is up to 61.2 %.

(2) Along with the increment of the thickness ratio of the viscoelastic layer to the hybrid fiber metal laminates ranging from 20 % to 70 %, the contact force peak in the load-displacement curves and displacement response perks are reduced by 46.0 % and 82.1%, which displays a downtrend of impact resistance and uptrend of anti-vibration property. Therefore, to keep a good balance of dynamic performance, it is recommended that the thickness ratio to be selected within a range of 30 % - 40 %.

(3) Since the improvement of Young's moduli of the viscoelastic layer has a limited influence on both vibration and impact properties of the overall plate structure, it is not recommended to increase the vibration and impact resistance via the adjustment of Young's moduli of the embedded viscoelastic material in the hybrid fiber metal laminates.

(4) The model proposed is not suitable for predicting high-velocity impact issues because the high strain rate effect and complex constitutive relationship is ignored. Meanwhile, its computational efficiency is slightly lower than that of general analytical model since it requires sufficient iterative calculations to solve dynamic responses. In the further research, the above problems need to be considered and improved, so that a more powerful integrated model can be established to assist in optimization design of hybrid fiber metal laminates embedded with a viscoelastic layer.

Acknowledgment

This study was supported by the National Natural Science Foundation of China (granted No. 51505070 and 11972204), the Fundamental Research Funds for the Central Universities of China (granted No. N180302004, N180703018, N180312012 and N180313006), the Science Foundation of the National Key Laboratory of Science and Technology on Advanced Composites in Special Environments (granted No. 6142905192512).

Declaration of Conflicting interests

The authors declare no potential conflicts of interest with respect to the research, authorship, and/or publication of this article.

References

[1] Lee D W, Park B J, Park S Y, Choi C H, Song J I. Fabrication of high-stiffness fiber-metal laminates and study of their behavior under low-velocity impact loadings. Compos Struct 2018;189:61-69.

[2] Zhu Q, Zhang C, Curiel-Sosa J L, Tinh Q B, Xu X J. Finite element simulation of damage in fiber metal laminates under high velocity impact by projectiles with different shapes. Compos Struct 2019;214: 73-82.

[3] Santiago R C, Cantwell W J, Jones N, et al. The modeling of impact loading on thermoplastic fiber-metal laminates. Compos Struct 2018;189:228-238.

[4] Li H, Xue P C, Guan Z W, Han Q K, Wen B C. A new nonlinear vibration model of fiber-reinforced composite thin plate with amplitude-dependent property. Nonlinear Dyn. 2018;94(3):2219-2241.

[5] Alderliesten R C, Homan J J. Fatigue and damage tolerance issues of Glare in aircraft structures. Int J Fatigue 2006;28(10):1116-1123.

[6] Li X, Zhang X, Guo Y B, Shim V P W, Yang J L, Chai G B. Influence of fiber type on the impact response of titanium-based fiber-metal laminates. Int J Impact Eng 2018;114 (APR.):32-42.

[7] Li H, Zhang T N, Li Z L, Wen B C, Guan Z W. Modeling of the nonlinear dynamic degradation characteristics of fiber-reinforced composite thin plates in thermal environment. Nonlinear Dyn. 2019; 98(1):819-839.

[8] Huang Z, Qin Z, Chu F. Vibration and damping characteristics of sandwich plates with viscoelastic core. J Vib Control 2014;22(7):1876-1888.

[9] Vlot A. Low-velocity impact loading on fibre reinforced aluminium laminates(ARALL) and other aircraft sheet materials. Delft University of Technology, 1991.

[10] Vlot A. Impact properties of fibre metal laminates. Compos Eng 1993;3(10):911-927.

[11] Vlot A. Impact loading on fibre metal laminates. Int J Impact Eng 1996;18(3):291-307.

[12] Vlot A, Kroon E, Rocca G L. Impact response of fiber mtal laminates. Key Eng Mater 1998;141-143:235-276.

[13] Khalili S M R, Shokuhfar A, Malekzadeh K, Ghasemi F A. Low-velocity impact response of active thin-walled hybrid composite structures embedded with SMA wires. Thin Wall Struct 2007;45(9):799-808.

[14] Shokuhfar A, Khalili S M R, Ghasemi F A. Analysis and optimization of smart hybrid composite plates subjected to low-velocity impact using the response surface methodology (RSM). Thin Wall Struct 2008;46(11):1204-1212.

[15] Payeganeh G H, Ghasemi F A, Malekzadeh K. Dynamic response of fiber-metal laminates (FMLs) subjected to low-velocity impact. Thin Wall Struct 2010;48(1):62-70.

[16] Guan Z W, Cantwell W J, Abdullah R. Numerical modeling of the impact response of fiber-metal laminates. Polym Composite, 2009;30(5):603-611.

[17] Zhou J, Hassan M Z, Guan Z W, Cantwell W J. The low velocity impact response of foam-based sandwich panels.

Compos Sci Technol 2012;72(14):1781-1790.

[18] Zhou J, Guan Z W, Cantwell W J. The impact response of graded foam sandwich structures. Compos Struct 2013;97(MAR.):370-377.

[19] Lin C, Fatt M S H. Perforation of composite plates and sandwich panels under quasi-static and projectile loading. J Compos Mater 2006;40(20):1801-1840.

[20] Morinière, F D, Alderliesten R C, Sadighi M, Benedictus R. An integrated study on the low-velocity impact response of the GLARE fibre-metal laminate. Compos Struct 2013;100:89-103.

[21] Morinière F D, Alderliesten R C, Benedictus R. Low-velocity impact energy partition in GLARE. Mech Mater 2013;66:59-68.

[22] Shooshtari A, Razavi S. A closed form solution for linear and nonlinear free vibrations of composite and fiber metal laminated rectangular plates. Compos Struct 2010;92(11):2663-2675.

[23] Fu Y M, Chen Y, Zhong J. Analysis of nonlinear dynamic response for delaminated fiber–metal laminated beam under unsteady temperature field. J Sound Vib 2014;333(22):5803-5816.

[24] Fu Y M, Shao X F. Dynamic Response of the Fiber Metal Laminated (FML) Plate with Interfacial Damage in Unstable Temperature Field. Appl Mech Mater 2014;490-491:403-411.

[25] Iriondo J, Aretxabaleta L, Aizpuru A. Dynamic characterisation and modelling of the orthotropic self-reinforced polypropylene used in alternative FMLs. Compos Struct 2016;153(oct.):682-691.

[26] Sessner V, Jackstadt A, Liebig W V, Karger L, Weidenmann K A. Damping characterization of hybrid carbon fiber elastomer metal laminates using experimental and numerical dynamic mechanical analysis. Compos Sci Technol 2019;3(1): 3-23.

[27] Nassir N A, Birch R S, Cantwell W J, Sierra D R, Guan Z W. Experimental and numerical characterization of titanium-based fibre metal laminates. Compos Struct 2020;245:112398.

[28] Malekzadeh K, Khalili M R, Olsson R, Jafari A. Higher-order dynamic response of composite sandwich panels with flexible core under simultaneous low-velocity impacts of multiple small masses. Int J Solids Struct 2006;43(22-23):6667-6687.

[29] Shariyat M, Hosseini S H. Eccentric impact analysis of pre-stressed composite sandwich plates with viscoelastic cores: A novel global-local theory and a refined contact law. Compos Struct 2014;117:333-345.

[30] Long S C, Yao X H, Wang H R, Zhang X Q. Failure analysis and modeling of foam sandwich laminates under impact loading. Compos Struct 2018;197:10-20.

[31] A L Araújo, Martins P, Soares C M M, Soares C A M, Herskovits J. Damping optimization of viscoelastic laminated sandwich composite structures. Struct Multidiscip O 2009;39(6):569-579.

[32] Azoti W L, Koutsawa Y, Bonfoh N, Lipinski P Belouettar S. Analytical modeling of multilayered dynamic sandwich composites embedded with auxetic layers. Eng Struct 2013;57(DEC.):248-253.

[33] Yang C M, Jin G Y, Ye X M, Liu Z G. A modified Fourier-Ritz solution for vibration and damping analysis of sandwich plates with viscoelastic and functionally graded materials. Int J Mech Sci 2016;106:1-18.

[34] Biswal D K, Mohanty S C. Free vibration study of multilayer sandwich spherical shell panels with viscoelastic core and isotropic/laminated face layers. Compos Part B-Eng 2019;72-85.

[35] Li H, Wang W Y, Wang X T Han Q K, Liu J G Qin Z Y, Xiong J, Guan Z W. A nonlinear analytical model of composite plate structure with an MRE function layer considering internal magnetic and temperature fields. Compos Sci Technol 2020.

[36] Li H, Wu H S, Zhang T N, Wen B C, Guan Z W. A nonlinear dynamic model of fiber-reinforced composite thin plate with temperature dependence in thermal environment. Compos Part B-Eng 2019;162:206-218.

[37] Hayes R L, Fago M, Michael O, Carte E A. Prediction of dislocation nucleation during nanoindentation of Al3Mg by the orbital-free density functional theory local quasicontinuum method. Philos Mag 2006;86(16):16.

[38] Zhang S Y, Tsai L W. Extending Tsai-Hill and norris criteria to predict cracking direction in orthotropic ma-terials. Int J Fatigue 1989;40(4):R101-R104.

[39] Dean G, Crocker L, Read B, Wright L. Prediction of de-formation and failure of rubber-toughened adhesive joints. Int J Adhes Adhe 2004;24(4):295-306.

[40] Wang Z X, Qiao P Z, Xu J F. Vibration analysis of laminated composite plates with damage using the perturbation method. Compos Part B-Eng 2015;72(apr.):160-174.

[41] Wu Q G, Wen H M, Qin Y, Xin S H. Perforation of FRP laminates under impact by flat-nosed projectiles. Compos Part B-Eng 2012;43(2):221-227.

[42] Fan, J, Guan, Z W, Cantwell W. J. Numerical modelling of perforation failure in fiber metal laminates subjected to low velocity impact loading, Compos Struct 2011;93(9): 2430-2436.

[43] Chen C, Sun C Z, Han X, Hu D A, Guan Z W. The structural response of the thermoplastic composite joint subjected to out-of-plane loading. Int J Impact Eng 2020:103691.

[44] Dragomiretskiy K, Zosso D. Variational Mode Decomposition. IEEE T Signal Proces 2014;62(3):531-544.

Appendix A

$$U_{\mathrm{M}} = \frac{1}{2}\int_A \int_{-h/2}^{-h/2+h_{\mathrm{m}}} \sum_{i=1}^{6} \sigma_{\mathrm{M}i}\varepsilon_{\mathrm{M}i} \mathrm{d}z\mathrm{d}A + \frac{1}{2}\int_A \int_{h/2\text{-}h_{\mathrm{m}}}^{h/2} \sum_{i=1}^{6} \sigma_{\mathrm{M}i}\varepsilon_{\mathrm{M}i} \mathrm{d}z\mathrm{d}A$$

$$T_{\mathrm{M}} = \frac{1}{2}\int_A \int_{-h/2}^{-h/2+h_{\mathrm{m}}} \rho_{\mathrm{M}} \left(\frac{\partial w}{\partial t}\right)^2 \mathrm{d}z\mathrm{d}A + \frac{1}{2}\int_A \int_{h/2\text{-}h_{\mathrm{m}}}^{h/2} \rho_{\mathrm{M}} \left(\frac{\partial w}{\partial t}\right)^2 \mathrm{d}z\mathrm{d}A$$

$$U_{\mathrm{F}} = \frac{1}{2}\int_A \int_{-h/2+h_m}^{-h_v/2} \sum_{i=1}^{6} \sigma_{\mathrm{F}i} \varepsilon_{\mathrm{F}i} \mathrm{d}z\mathrm{d}A + \frac{1}{2}\int_A \int_{h_v/2}^{h_f+h_v/2} \sum_{i=1}^{6} \sigma_{\mathrm{F}i} \varepsilon_{\mathrm{F}i} \mathrm{d}z\mathrm{d}A$$

$$T_{\mathrm{F}} = \frac{1}{2}\int_A \int_{-h/2+h_m}^{-h_v/2} \rho_{\mathrm{F}} \left(\frac{\partial w}{\partial t}\right)^2 \mathrm{d}z\mathrm{d}A + \frac{1}{2}\int_A \int_{h_v/2}^{h_f+h_v/2} \rho_{\mathrm{F}} \left(\frac{\partial w}{\partial t}\right)^2 \mathrm{d}z\mathrm{d}A$$

$$U_{\mathrm{V}} = \frac{1}{2}\int_A \int_{-h_v}^{h_v} \sum_{i=1}^{6} \sigma_{\mathrm{V}i} \varepsilon_{\mathrm{V}i} \mathrm{d}z\mathrm{d}A$$

$$T_{\mathrm{V}} = \frac{1}{2}\int_A \int_{h_v}^{-h_v} \rho_{\mathrm{V}} \left(\frac{\partial w}{\partial t}\right)^2 \mathrm{d}z\mathrm{d}A$$

where $\sigma_{\mathrm{m}i}$, $\sigma_{\mathrm{f}i}$, $\sigma_{\mathrm{v}i}$ are the stresses of metal layers, fiber layers and viscoelastic layer, respectively; $\varepsilon_{\mathrm{m}i}$, $\varepsilon_{\mathrm{f}i}$, $\varepsilon_{\mathrm{v}i}$ are the corresponding strains; ρ_{m}, ρ_{f}, ρ_{v} are the corresponding densities, A is the area of the VC-FML plate.

Appendix B

Table B1. Values of δ_q and ψ_{ij}^q related to the q-th failure event

Failure type	δ_q	ψ_{11}^q	ψ_{12}^q	ψ_{22}^q	ψ_{44}^q	ψ_{55}^q	ψ_{66}^q
Metal layer	0.25	1	1	1	1	1	1
Composite layer	0.06	1	2	3	1.5	1.5	1.5
Viscoelastic layer	0.02	1	1	1	1.2	1.2	1.2